Urban Forestry & Urban Greening 107 (2025) 128785

Contents lists available at ScienceDirect

Urban Forestry & Urban Greening

journal homepage: www.elsevier.com/locate/ufug

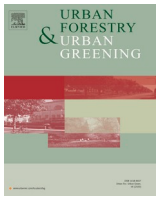

Original article

Urban green space vegetation height modeling and intelligent classification based on UAV multi-spectral and oblique high-resolution images

Ronghua Li [a], Zhican Bai [b,c], Chao Ye [d], Sergey Ablameyko [e], Shiping Ye [b,c,*]

[a] School of Information Engineering, Huzhou University, Huzhou 313000, China
[b] School of Information Science and Technology, Zhejiang Shuren University, Hangzhou 310015, China
[c] International Science and Technology Cooperation Base of Zhejiang Province: Remote Sensing Image Processing and Application, Hangzhou 310015, China
[d] Hangzhou Hikrobot Co., Ltd, Hangzhou 310000, China
[e] Belarusian State University, 4, Nezavisimosti Ave, Minsk 220030, Belarus

ARTICLE INFO

Keywords:
Urban green space
Remote sensing
Unmanned aerial vehicle
Oblique photography
Intelligent classification
Canopy height model

ABSTRACT

Urban green space (UGS) vegetation plays an important role in mitigating the urban heat island effect by improving the environment and quality of life. Hence, there is a dire necessity for urban planning and management to precisely obtain the spatial distribution and structural information employing high-resolution data. Nevertheless, the limitations of remote sensing (RS) data and the complexity of urban landscapes pose significant challenges, so this study aims to introduce a method to classify UGS vegetation more precisely by integrating high spatial resolution multi-spectral and oblique photography images captured by unmanned aerial vehicle (UAV). A novel canopy height model (CHM) method is proposed to generate UGS vegetation information for urban areas while addressing the errors associated with traditional approaches in estimating non-ground vegetation heights, achieving a total Mean Absolute Error (MAE) of 0.17 m and an overall accuracy of 95.03 %. The proposed UGS mapping method combines spectral features, canopy height information, vegetation indices (VIs), and texture features to evaluate the impact of various characteristics on classification accuracy. The obtained experimental results show that by incorporating canopy height information classification accuracy is significantly improved and achieve overall accuracy of 93.82 % and Kappa coefficient of 0.91. Moreover, the proposed method not only precisely reflects the structure and distribution of UGS vegetation by showing specific advantages in complex environments but also offers a new arena for UGS vegetation classification based on the integration of multiple features.

1. Introduction

With significant ecological advantages like enhancing air quality, reducing the heat island effect, and maintaining biodiversity, urban green space (UGS) is essential to urban ecosystems (Chen et al., 2017). Furthermore, UGS provides inhabitants with essential social and recreational areas that support mental stress reduction and the preservation of both physical and mental well-being (Yang et al., 2018). As climate change intensifies, vegetation within UGS has become increasingly important in mitigating urban carbon emissions, functioning as long-term carbon storage (Zhao et al., 2023; Zhuang et al., 2022). However, in the process of global rapid urbanization, large areas of agricultural and forest land have been converted into impermeable concrete surfaces, leading to a continuous decline in vegetation coverage and increasing fragmentation of ecosystems (Chen et al., 2018; Nero, 2017; Richards and Belcher, 2019). Due to above mentioned phenomenon that has brought severe impacts on the environment and human health it has been imperative to carry out the effective planning and management of UGSs by exploring new technologies to enhance the ecological services of UGSs to achieve sustainable development goals (SDGs).

In recent years, the rapid development of remote sensing (RS) technologies has provided new methods for monitoring UGS vegetation (Kopecká et al., 2017; Neyns and Canters, 2022). The RS enables timely acquisition of information on the distribution and trends of UGSs, thereby helping policymakers to make informed decisions regarding UGS planning and management in order to address environmental challenges associated with urban expansion (Di et al., 2019; Jiang et al.,

* Corresponding author at: School of Information Science and Technology, Zhejiang Shuren University, Hangzhou 310015, China.
E-mail addresses: ysp@zjsru.edu.cn, zjsruysp@163.com (S. Ye).

https://doi.org/10.1016/j.ufug.2025.128785
Received 13 December 2024; Received in revised form 8 February 2025; Accepted 16 March 2025
Available online 19 March 2025

2024). Current research studies have chiefly relied on the medium- and high-resolution satellite imagery for UGS mapping, but there is relatively little research on utilizing high-resolution multi-source UAV-based RS (Sathyakumar et al., 2019; Wang et al., 2024). Gašparović and Dobrinić (2020) evaluated and compared the machine learning methods for classifying European urban vegetation using multi-temporal Sentinel-1 SAR imagery, their results indicated that multi-temporal data significantly improved classification accuracy. The widespread applications of UAV RS technology have demonstrated their unique advantages in vegetation monitoring (Behera et al., 2023; Feng et al., 2015; Sotille et al., 2020). Bhatnagar et al. (2020) utilized UAV imagery for image segmentation of vegetation in the Clara Bog wetlands in Ireland by comparing machine learning and deep learning algorithms which showed that the random forest (RF) classifier and the ResNet50 +SegNet model performed best. The deep learning achieved higher accuracy, but it required extensive training data and computational resources, making machine learning classifiers more suitable for specific wetland vegetation applications in terms of cost and efficiency. Onishi and Ise (2021) developed a low-cost system using UAV-based RGB imagery to successfully classify trees with an accuracy of over 90 % by providing an effective tool for forest management.

The high resolution and flexibility in data acquisition offered by UAV imagery present a promising solution for precise studies of UGS vegetation. However, in urban environments, the diversity and uneven distribution of vegetation types pose significant challenges for rapid and accurate vegetation mapping (Xu et al., 2020). Different types of vegetation often exhibit similar spectral characteristics, making it difficult to accurately classify them based on spectral information alone (Zhao et al., 2021). Thus, selecting appropriate variables is critical for accurate vegetation classification, particularly when using multi-source RS data (Radke et al., 2020; Xie et al., 2019). Recent studies have focused on evaluating the value of auxiliary information in vegetation classification, such as texture and height data, as these features can significantly enhance classification accuracy (Chiang and Valdez, 2019; Liu et al., 2017; Yu et al., 2020). For instance, Prošek and Šímová (2019) integrated multi-spectral data with vertical information obtained from UAV to achieve species-level classification of shrub vegetation, their results demonstrated that the fusion method yielded higher accuracy than using multi-spectral data alone. Komárek et al. (2018) combined multi-spectral, thermal, and height data from UAV for fine vegetation classification, showing that height and thermal data significantly improved classification accuracy, demonstrating the potential of drone technology in classifying complex vegetation areas. Murray et al. (2010) were the first to use high-resolution IKONOS imagery to classify vegetation communities on Heard Island, an Antarctic sub-island, and their results revealed that integrating texture features with multi-spectral data effectively improved classification accuracy.

One of the Several emerging RS technologies i.e., light detection and ranging (LiDAR) can accurately measure surface and vegetation heights but it is expensive and requires specialized sensors (Gillan et al., 2014). In contrast, measuring vegetation height using digital stereoscopic aerial photographs, such as oblique photogrammetry, offers a more economical and feasible alternative (Che et al., 2020). The canopy height model (CHM) is commonly used for describing vegetation height information, typically calculated as the difference between the digital surface model (DSM) and the digital terrain model (DTM) (Granholm et al., 2015; Kothencz et al., 2018). However, in densely built urban environments, traditional CHM calculation methods encounter certain issues due to the demand for beautifying spaces or alleviating stress and many building surfaces or rooftops are utilized for greening, resulting in a large amount of non-ground-level green landscapes in urban areas. The conventional calculation methods may incorrectly attribute building heights to vegetation heights, leading to significant errors in the actual values and it can also affect the accuracy of classification results, and such errors amplify in the high-resolution UAV imagery. Moreover, the limited penetration capability of oblique photogrammetry makes it difficult to obtain information beneath the canopy in the form of a DTM, further complicating the accurate acquisition of CHM (Lisein et al., 2013). Therefore, it necessitates a dire need to develop effective methods to generate CHM in the urban environments.

The previous conducted studies have made numerous attempts to monitor UGS vegetation using RS technology (Shahtahmassebi et al., 2021; Wang et al., 2021), however, research on combining high-resolution multi-spectral imagery and oblique photogrammetry from UAV to extract canopy height information and classify UGS vegetation remains limited, and its efficiency necessitates further validation. The proposed paper successfully fills the research gap left in the literature review and the main contribution of the study are stated below:

- This study aims to enhance the classification of UGS vegetation using high-resolution multi-spectral and oblique photogrammetry UAV imagery.
- A method for CHM construction is proposed, which is suitable for urban areas and addresses the errors in traditional methods for estimating non-ground vegetation heights.
- Additionally, an object-based classification approach is employed, combining spectral features, canopy height information, vegetation indices (VIs), and texture features to evaluate the impact of different variables on the accuracy of UGS vegetation classification.
- This research offers new insights into the precise classification of UGS vegetation and provides scientific evidence to promote sustainable urban development.

The rest of the paper is followed by Section 2 describing the details of the study area and proposed method. Section 3 gives the details of experiments and results obtained from the simulations. The detailed discussion is given in Section 4. Finally, Section 5 concludes this paper and provides some ideas for future research.

2. Materials and methods

2.1. Study area

The study area is located in the northeastern part of Hangzhou, in Zhejiang Province, China which is a modern city characterized by economic dynamism and cultural prosperity. The geographical co-ordinates of the study area are 30°19′N latitude and 120°9′E longitude, as shown in Fig. 1. The area covers the main part of the Gongchenqiao, South Campus of Zhejiang Shuren University, with a total area of approximately 147,776 square meters (14.77 ha). This moderate-scale region provides an ideal setting for in-depth research on the distribution and types of UGS vegetation. The study area is situated at the heart of the city, and it is not only densely populated and commercially developed but also rich in historical and cultural heritage. The typical urban environment of this area offers a unique backdrop for vegetation studies, making the research results not only regionally representative but also broadly applicable.

2.2. Technology Roadmap

Fig. 2 illustrates the technical workflow of the proposed study. The main work can be divided into two parts.

In the first part, a vegetation CHM modelling method suitable for urban areas is proposed. The proposed method consists of three main stages: (1) vegetation extraction; (2) rapid generation of the DTM based on the DSM derived from oblique photogrammetry; and (3) generation of the CHM based on the corrected vegetation height. While in the second part, this study utilizes high-resolution dual-source UAV imagery combined with object-based image analysis and feature extraction and selection techniques for detailed classification of UGS vegetation. The proposed method includes six steps: (1) determining the optimal segmentation parameters and performing image segmentation; (2) deriving

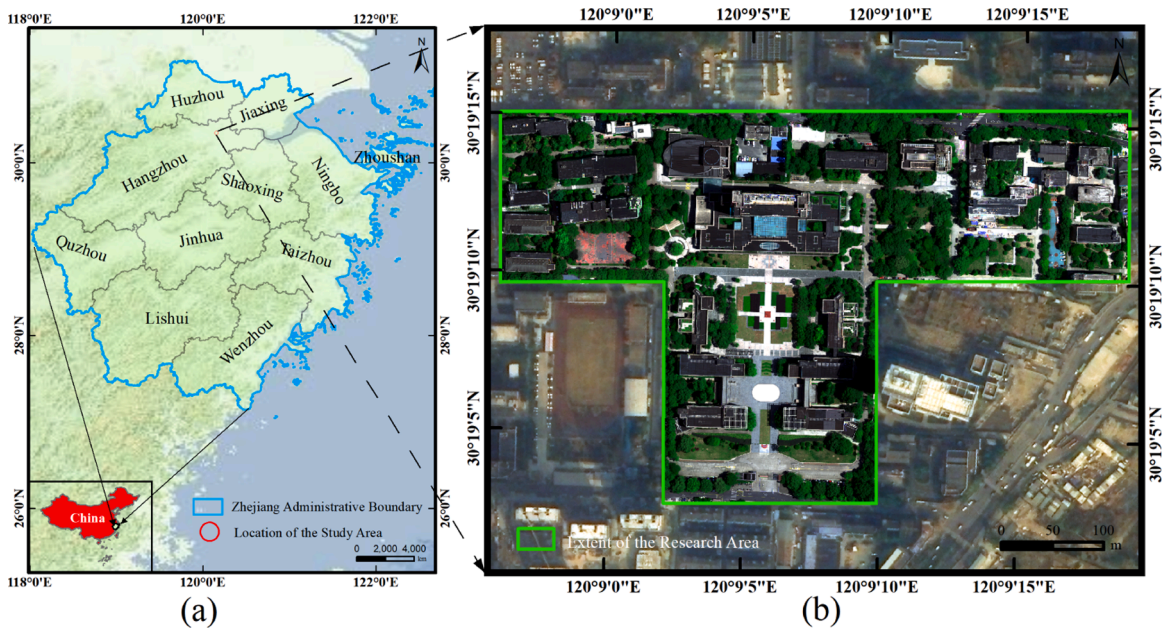

Fig. 1. Map of the study area. (a) Location; (b) Digital orthophoto images.

48 key features from dual-source UAV imagery and developing classification schemes based on different feature sets; (3) applying the object-based RF model for vegetation classification; (4) evaluating the accuracy of different classification schemes; (5) assessing the contribution of different feature types and the effectiveness of feature selection; and (6) implementing vegetation classification of UGS in the study area.

2.3. UAV image acquisition and preprocessing

In this study, high-resolution dual-source UAV imagery comprising multi-spectral and oblique photogrammetry data was collected. The multi-spectral imagery provided rich vegetation reflectance information, revealing the physiological characteristics of the vegetation while the oblique photogrammetry data provided multi-angle image data, reflecting the spatial distribution and morphological features of UGS vegetation.

Data collection was conducted using the DJI Matrice 300 RTK UAV, equipped with the MicaSense RedEdge MX camera for multi-spectral imaging. This camera captured five spectral bands: blue, green, red, red edge, and near-infrared. For oblique photogrammetry, the PSDK 102S V3 camera was used. Detailed camera parameters are provided in Table 1. The image acquisition was conducted on May 14, 2024, and specific flight parameters are listed in Table 2.

The study utilized Pix4Dmapper to produce digital orthophoto maps (DOMs), with an image GSD of 8 cm/px. For the oblique photogrammetry data, project files automatically generated by ShareElf software were imported into Context Capture for 3D modeling. These block files contained the relevant photo data. The DSM was subsequently generated utilizing Context Capture, with the same resolution as the DOM.

2.4. Method for constructing urban green canopy height models based on dual-source UAV remote sensing imagery

2.4.1. Vegetation extraction

This study employs multi-spectral orthophoto imagery to calculate VI for extracting vegetation regions. Given the suitability of the RS imagery in the study area, the Moderate Red-edge Vegetation Index (MREVI) (Li et al., 2024) was chosen for extracting UGS vegetation information. The formula is as follows:

$$\mathrm{MREVI} = 100 \times \frac{(\max(\mathrm{RE},\mathrm{NIR}) - \max(\mathrm{RED},\mathrm{RE})) \times (\min(\mathrm{RE},\mathrm{NIR}) - \min(\mathrm{RED},\mathrm{RE}))}{(\mathrm{RED}+\mathrm{RE}+\mathrm{NIR})^2} \times \frac{\mathrm{RE}-\mathrm{RED}}{\mathrm{RE}+\mathrm{RED}} \times \mathrm{NIR} \quad (1)$$

Where RED, RE and NIR represent the reflectance in the red, red-edge and near-infrared spectral bands respectively.

After calculating the VI, a binarization process is applied to the image to generate a vegetation mask (Viani et al., 2024b), marking vegetation areas as the foreground (value = 1) and other areas as the background (value = 0). The binarization formula is:

$$\mathrm{M_{veg}}(x,y) = \begin{cases} 1, & \mathrm{MREVI} > \tau \\ 0, & \mathrm{MREVI} < \tau \end{cases} \quad (2)$$

Where $\mathrm{M_{veg}}(x,y)$ represents the binary vegetation mask image, and τ is the classification threshold between vegetation and the background.

2.4.2. Urban digital terrain model

The urban digital terrain model (DTM) is a 3D model representing the elevation of the earth's surface, excluding objects such as vegetation and buildings (Dai et al., 2020) and an accurate DTM is critical for obtaining vegetation canopy height data. Based on the characteristics of urban terrain, the Inverse Distance Weighting (IDW) interpolation method (Watson, 1985) was taken to efficiently generate DTM by processing the DSM.

Since the terrain is relatively flat in urban areas, adjacent surface elevation values change minimally and it allows the retention of surface

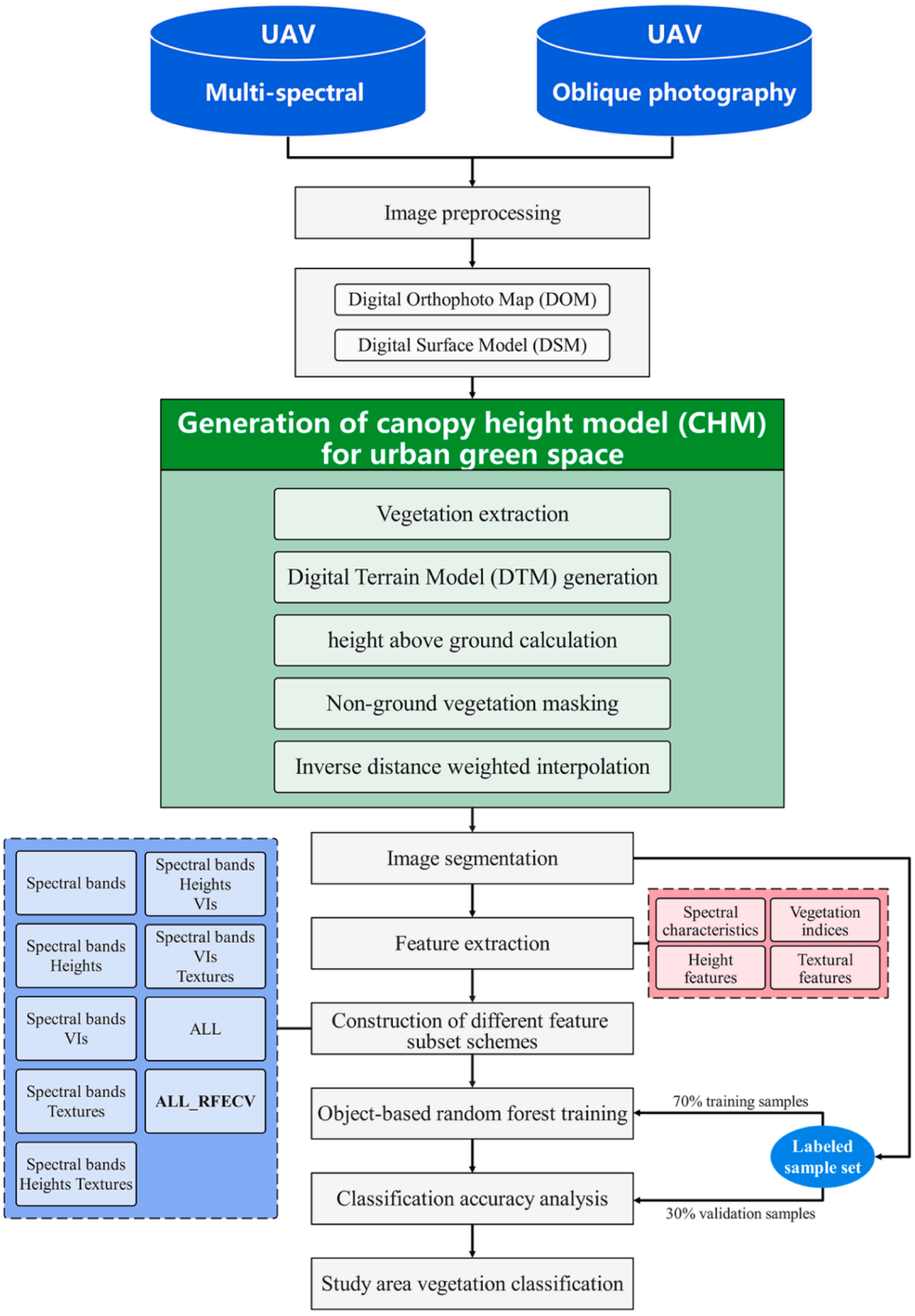

Fig. 2. Technical flow chart.

Table 1
Specifications of the Micasense RedEdge MX and the PSDK 102S V3.

Sensor	Resolution	GSD at 100 m (cm/px)	Pixel size	Sensor size	Focal length
RedEdge MX	1280 × 960 (1.2 MP×5 bands)	6.9	3.75 μm	4.8 mm× 3.6 mm	5.4 mm
PSDK 102S V3	6144 × 4096 (25.16 MP×5 views)	1.5	3.76 μm	23.1 mm× 15.4 mm	25 mm

Table 2
Basic parameters of the flight missions.

Sensor	Speed (m/s)	Height (m)	Overlap (%)	Gained images	Aligned images
RedEdge MX	15	115	80	1158	1158
PSDK 102S V3	14.7	100	75	965	907

elevation values through interpolation to represent the actual topography of the study area. Firstly, a mask was applied to non-surface areas to retain the surface elevation values of other regions and the vegetation

extraction results were used to retain the non-vegetation area elevation values in the DSM.

$$\mathrm{DSM}_{\mathrm{non-veg}}(x,y) = \mathrm{DSM}(\mathrm{x},\mathrm{y}) \times \left(1 - \mathrm{M}_{\mathrm{veg}}(x,y)\right) \tag{3}$$

Where $\mathrm{DSM}(x,y)$ is the original Digital Surface Model, $\mathrm{M}_{\mathrm{veg}}(x,y)$ is the vegetation mask, and $\mathrm{DSM}_{\mathrm{non-veg}}(x,y)$ is the elevation value for non-vegetation areas.

These elevation values contain both surface and building elevation data and based on the range of surface elevations, points where $\mathrm{DSM}_{\mathrm{non-veg}}(x,y) > \mathrm{T}$ were considered non-surface elevations and masked. The remaining DSM values were considered surface elevations and used to generate DTM through interpolation. By retaining only surface elevation values, an initial DTM was obtained:

$$\mathrm{DTM}_{\mathrm{initial}}(x,y) = \begin{cases} \mathrm{DSM}_{\mathrm{non-veg}}(x,y) & \text{if } \mathrm{DSM}_{\mathrm{non-veg}}(\mathrm{x},\mathrm{y}) < \mathrm{T} \\ 0 & \text{else} \end{cases} \tag{4}$$

Next, the IDW method was applied to the masked areas to estimate and fill the surface elevation values of masked regions.

$$d_{pj} = \sqrt{\left(x_p - x_j\right)^2 + \left(y_p - y_j\right)^2} \tag{5}$$

$$\mathrm{DTM}_{\mathrm{Interpolated}}(x,y) = \frac{\sum_{j=1}^{n} \frac{h_j}{d_{pj}^k}}{\sum_{j=1}^{n} \frac{1}{d_{pj}^k}} \tag{6}$$

Where (x_p, y_p) represents the interpolation point, (x_j, y_j) represents the known point, d_{pj} is the distance between the interpolation point and the known point, h_j represents the known elevation, n is the number of known points, and k is the weighting exponent, usually set to 2 (Liu et al., 2021).

2.4.3. Generation of the urban green canopy height model

In order to address errors in conventional CHM calculation methods, this study proposes an improved method for constructing the CHM for UGS by retaining only the height of UGS vegetation and correcting the height of non-ground vegetation.

A. Above-ground height calculation

In this study, the difference between DSM and DTM is used to calculate the above-ground height (HAG), representing the height of objects above the local ground. The formula for calculating HAG is:

$$\mathrm{HAG}(x,y) = \mathrm{DSM}(x,y) - \mathrm{DTM}(x,y) \tag{7}$$

B. Non-ground vegetation extraction and masking

The connected component analysis is applied to the binarized vegetation mask image to extract all connected regions where each k-th connected region R_k can be represented as:

$$R_k = \{(x,y) | L(x,y) = k\} \tag{8}$$

$L(x,y)$ is a label image, retaining the region label of each pixel. The morphological dilation is performed on each connected region R_k, with a given dilation radius r, resulting in an expanded region D_k:

$$D_k = \{(x',y') | \exists (x,y) \in R_k \text{ and } \sqrt{(x'-x)^2 + (y'-y)^2} \le r\} \tag{9}$$

For each connected vegetation region, an outer annular region O_k is obtained, which is the difference between the expanded region and the original connected region:

$$O_k = D_k \backslash R_k \tag{10}$$

The height values of the outer annular region are checked to determine whether they meet ground height characteristics. If the outer annular region shows non-ground height then the identified non-ground vegetation regions are masked by retaining only the ground height values:

$$\mathrm{M}_{\mathrm{ng-veg}}(x,y) = \begin{cases} 1 & \text{if } (x,y) \in R_k \text{ and } O_k \text{ is not ground} \\ 0 & \text{else} \end{cases} \tag{11}$$

$$\mathrm{HAG}_{\mathrm{masked}}(x,y) = \mathrm{M}_{\mathrm{ng-veg}}(x,y) \bullet \mathrm{HAG}(x,y) \tag{12}$$

C. Non-ground vegetation canopy height correction

Similar to DTM interpolation, the IDW method is applied to the masked regions. Based on the HAG values of the surrounding surfaces, the canopy height of non-ground vegetation is filled, ensuring the canopy height represents the true vegetation height rather than the height relative to the ground.

$$\mathrm{HAG}_{\mathrm{Interpolated}}(x,y) = \frac{\sum_{j=1}^{n} \frac{h_j}{d_{pj}^k}}{\sum_{j=1}^{n} \frac{1}{d_{pj}^k}} \tag{13}$$

D. Canopy Height Model Generation

For the ground vegetation, the CHM is obtained from the difference of DSM and DTM, i.e., the HAG and for the non-ground vegetation regions, the CHM is obtained from the IDW interpolation result. The CHM is stored in raster form as follows:

$$\mathrm{CHM}(x,y) = \begin{cases} \mathrm{HAG}(\mathrm{x},\mathrm{y}) & \mathrm{M}_{\mathrm{veg}}(x,y) = 1 \text{ and } \mathrm{M}_{\mathrm{ng-veg}}(x,y) = 0 \\ \mathrm{HAG}_{\mathrm{Interpolated}}(x,y) & \mathrm{M}_{\mathrm{veg}}(\mathrm{x},\mathrm{y}) = 1 \text{ and } \mathrm{M}_{\mathrm{ng-veg}}(x,y) = 1 \\ 0 & \mathrm{M}_{\mathrm{veg}}(x,y) = 0 \end{cases} \tag{14}$$

2.5. Object-based vegetation classification integrating multiple features

2.5.1. Image segmentation

The use of object-based techniques for high spatial resolution RS image categorization has grown in recent years (Katz et al., 2020). Object-based approaches to land cover categorization are more accurate than conventional pixel-based approaches (Snavely et al., 2019). The ability of the object-based approach is to accurately capture the spatial properties and structural information of homogeneous regions in the image (Pu et al., 2011).

The image segmentation is a key step in object-based classification, as its results directly impact the classification accuracy. Trimble eCognition Developer 10.3 software was effectively used for image segmentation utilizing a multi-resolution segmentation algorithm. During the segmentation process, the true-color orthophotos from oblique photography and the DSM were used as input layers while the segmentation of land cover areas was based on the integration of color, texture, and height information. The multi-resolution segmentation algorithm included four important parameters: layer weight, scale, shape index, and compactness. The segmentation parameter settings significantly influenced the segmentation outcome. For instance, the scale determines the size of the segmentation objects: a larger scale produces fewer and larger objects but might miss details, while a smaller scale generates more and smaller objects, which could lead to over-segmentation. After repeated experiments and visual comparisons through different parameter combinations, the optimal combination was determined as layer weights = [1, 1, 1, 2], scale parameter = 80, shape index = 0.2, and compactness = 0.7. After executing the segmentation, 121,648 polygon vector areas of varying resolutions were obtained from the raster images.

2.5.2. Reference data

The obtained segmentation results were converted into the industry-standard ESRI Shapefile format to obtain training and testing samples. These polygons were overlaid on high-resolution true-color orthophotos from oblique photography and combined with 3D real-scene models for manual visual interpretation where sample labelling was performed using ArcGIS 10.8, assigning each polygon to a specific category. During the labelling process, special attention was given to factors like shadows and occlusion that could affect visual interpretation and field checks

Table 3
The distribution of samples for primary greening types in the research area.

Classes	Number of polygons	Area (m^2)	Percentage (%)
Grass	6251	12088.90	8.18
Shrub	3269	5804.62	3.92
Tree	50739	50055.21	33.87
Building	25936	34718.32	23.49
Background	35453	45109.51	30.52
All	121648	147776.59	100

were carried out to ensure each region was accurately labelled. Through visual referencing and verification, each polygon object was categorized and this study considered common types in UGSs, including grass, shrub, tree, building, and background areas, as shown in Table 3. In terms of distribution, three category objects were the most prominent, while the proportions of shrub and grass objects were similar.

This study employs a stratified sampling method to construct both the training dataset and the validation dataset, ensuring that the proportion of each category in both datasets is consistent. For each category, a 7:3 random sampling ratio was used, with 13,098 polygons serving as training samples for training the classification model and 5614 polygons used to validate classification accuracy.

2.5.3. Feature extraction

The integration of multiple type features can improve the separability of vegetation types (Franklin et al., 2000), hence, in addition to spectral features, this study also extracted the height information, VIs, and texture features to analyze the contribution of different feature types to UGS vegetation classification.

1. **Spectral features:** It is derived from the reflectance of five multispectral bands (blue, green, red, red edge, and near-infrared) and the digital number (DN) values of three bands from oblique photography (red, green, and blue) to calculate the mean and standard deviation of each band.
2. **Height information:** It includes the mean, and standard deviation of DSM and CHM.
3. **Vegetation indices**: The vegetation indices are known for the sensitivity to vegetation growth and biomass and this study calculated four common spectral VIs, as listed in Table 4.
4. **Texture features:** These features are extracted from high-resolution oblique photography images and DSM and this study computed 20 typical texture variables (Haralick et al., 1973), including Energy (ENE), Contrast (CON), Entropy (ENT), Correlation (COR), and Inverse Difference Moment (IDM). The formulas and applications of these texture features are detailed in Table 5.

2.5.4. Supervised classifier

Vegetation objects segmented at different scales by means of the multi-resolution segmentation were treated as the smallest classification units for the supervised classification of UGS vegetation. Random Forest (RF) is an ensemble learning method that improves the accuracy and robustness by constructing multiple decision trees (Belgiu and Drăguţ, 2016). Different from the traditional classification models with poor generalization capabilities, RF significantly enhances classification accuracy, reduces the impact of outliers, and prevents overfitting. Specifically, it generates multiple sub-sample sets through bootstrapping and then trains a decision tree on each subsample and at each node during training, RF randomly selects a subset of features to split to increase model diversity. Eventually, RF obtains the final prediction result through a voting process (for classification tasks) among all decision trees and this method effectively reduces the overfitting issues associated with single decision trees and improves overall predictive performance and generalization. RF performs exceptionally well when dealing with high-dimensional data and tasks with complex decision boundaries and offers good interpretability and flexible parameter tuning.

Table 4
Vegetation indices (VIs) and applications.

Vegetation Indices	Formulation	Reference
NDVI	$\frac{NIR - RED}{NIR + RED}$	Rouse et al., 1974
$NDVI_{rededge}$	$\frac{RE - RED}{RE + RED}$	Timmer et al., 2022
EVI	$2.5 \times \frac{NIR - RED}{NIR + 6 \times RED - 7.5 \times BLUE + 1}$	Huete et al., 2002
SAVI	$1.5 \times \frac{NIR - RED}{NIR + RED + 0.5}$	Huete, 1988

Table 5
Texture metrics and applications.

Texture Metrics	Formulation	Application
ENE	$\sum_{i,j} P(i,j)^2$	Measuring the uniformity and texture coarseness of gray levels in images
CON	$\sum_{i,j} (i-j)^2 P(i,j)$	Measuring the degree of local variation in gray levels within images
ENT	$-\sum_{i,j} P(i,j) \log P(i,j)$	Measuring the complexity and disorder of texture distribution
COR	$\frac{\sum_{i,j}(i-\mu_i)(j-\mu_j)P(i,j)}{\sigma_i \sigma_j}$	Measuring the linear relationship between pixel gray levels
IDM	$\sum_{i,j} \frac{P(i,j)}{1+(i-j)^2}$	Measuring the local similarity of images

2.5.5. Construction of different feature subsets

This study used 48 features comprising raw image bands, VIs, texture metrics, and height information, as inputs for the RF classifier to accurately distinguish vegetation types. In order to explore the contribution of different types of features and their impact on classification results, different object-based feature subsets were designed, forming nine classification schemes for UGS vegetation, as shown in Table 6. This study evaluated the contribution of different types of features to the classifier by incrementally adding spectral features, height information, VIs, and texture features. S1 contained only spectral features, S2 added height features based on oblique photography, S3 added VIs based on spectral information, and S4 included texture features. S5 and S6 added VIs and texture features to S2, respectively. S7 added texture features to S3, and S8 included all feature types.

Feature selection plays a key role in object-based classification and several studies have shown that redundant features can negatively impact the performance and stability of classification models (Shi et al., 2021), therefore, it is necessary to optimize and reduce the number of features by eliminating irrelevant ones. Recursive Feature Elimination with Cross-Validation (RFECV) is a method used in machine learning to optimize feature selection (HARIF and KASSIMI, 2024) as it recursively removes features that contribute the least to the model and applies cross-validation at each step to evaluate the performance of feature subsets, thereby determining the feature set that most improves generalization capability of the model and the optimal feature subset, S9, was selected using the RFECV method.

2.5.6. Evaluation metrics

In order to determine the optimal UGS vegetation classification scheme based on UAV dual-source imagery and analyze the effectiveness of different feature types, this study used confusion matrix-related metrics to evaluate the accuracy of the vegetation classification. Specifically, this study calculated the four key metrics along with their related calculation expressions are given as follows:

(1) Overall Accuracy (OA):

Table 6
Nine object-based classification feature subsets schemes design.

Schemes	Classification features	Spectral	Heights	VIs	Textures	Total features
S1	Spectral bands	16				16
S2	Spectral bands + Heights	16	4			20
S3	Spectral bands + VIs	16		8		24
S4	Spectral bands + Textures	16			20	36
S5	Spectral bands + Heights + VIs	16	4	8		28
S6	Spectral bands + Heights + Textures	16	4		20	40
S7	Spectral bands + VIs + Textures	16		8	20	44
S8	ALL	16	4	8	20	48
S9	ALL_RFECV	7	4	3	3	17

$$OA = \frac{\sum_{i=1}^{k} C_{ii}}{N} \tag{15}$$

(2) Producer Accuracy (PA):

$$PA_i = \frac{C_{ii}}{\sum_{j=1}^{k} C_{ij}} \tag{16}$$

(3) User Accuracy (UA):

$$UA_i = \frac{C_{ii}}{\sum_{j=1}^{k} C_{ji}} \tag{17}$$

(4) Kappa Coefficient:

$$k = \frac{P_o - P_e}{1 - P_e} \tag{18}$$

where C_{ii} is the element on the diagonal of the error matrix (i.e., the number of correctly classified samples), N is the total number of pixels, k is the number of categories, P_o is the observed agreement probability, and P_e is the expected agreement probability.

3. Experiments and results

3.1. Experimental environment and process

The experimental environment for this study consisted of a Lenovo ThinkSystem SR650 server, configured with two Intel Xeon Gold 5117 CPUs @ 2.00 GHz, 256 GB DDR4 memory (2666 MHz), and an NVIDIA Tesla V100 GPU (32 GB). The additional software included Python 3.8, ENVI 5.3, ArcGIS 10.3, Trimble eCognition Developer 10.3, and ContextCapture 10.2.

The experimental process of this study included the following steps: (1) Vegetation extraction was initially conducted with the MREVI derived from multi-spectral imaging to differentiate vegetation from non-vegetation zones in the study area. Based on previous studies (Li et al., 2024), the threshold value for MREVI was set at 0.1, which achieved the best vegetation extraction results for the study area. (2) The CHM for UGS was produced using a vegetation canopy height correction technique that relies on dual-source imagery to get height data for UGS vegetation. (3) Image segmentation was performed via eCognition software, wherein segmentation algorithms partitioned the imagery into multiple items to enable subsequent classification analysis. (4) Features were extracted for each segmented object, encompassing spectral features, height features, vegetation indices, and texture features, and feature sets were assembled for training the classification model. (5) An object-based RF model was trained by optimizing the classification process. A configuration of 200 trees (ntree = 200) was selected, and the mtry parameter was assigned its default value, which is the square root of the total number of features. Feature selection was implemented using RFECV, which iteratively removed the least important features based on their contribution to model performance. The RFECV process utilized 3-fold cross-validation and selected the optimal subset of 17 features, achieving a balance between model accuracy and computational efficiency. (6) The UGS vegetation in the study area was classified based on the trained model by generating accurate classification results to analyze the spatial distribution characteristics of UGS.

3.2. Urban green space canopy height model

Two typical local areas with non-ground vegetation were selected to verify the effectiveness of the proposed method for generating the CHM based on UAV dual-source RS imagery, as shown in Fig. 3.

Fig. 3(a) and (d) illustrate the HAG obtained from the difference between DSM and DTM where the proposed approach not only yields above-ground height data but also incorporates the height of non-vegetative regions which results in interference. In Fig. 3(b) and (e), non-vegetation height data were obscured to eliminate non-vegetation effects, yet some substantial problems persisted. Certain non-ground vegetation heights were mistakenly computed as significantly bigger than their true values due to calculations being based on ground-relative height. The traditional CHM calculating method finally proved to be ineffective for metropolitan regions. Fig. 3(c) and (f) depict the outcomes of the proposed strategy where this method produces a CHM that exclusively incorporates the genuine canopy heights of plants which correctly represents the actual height of the vegetation.

To verify the accuracy and reliability of the CHM generation, this study evaluated it using ground-based measured data. The ground validation data was collected using a high-precision handheld altimeter (accuracy ± 0.1 m) and Real-Time Kinematic (RTK) positioning equipment (accuracy ± 0.01 m). Within the study area, representative plots were selected, covering different vegetation types (such as trees, shrubs, and grasslands) and terrain conditions (including ground vegetation and non-ground vegetation). For each terrain condition, five measurement points were evenly distributed across each category to ensure spatial distribution rationality. During the measurement process, the vertical height from the tree crown top to the ground was measured using the altimeter for trees, while a tape measure was used to directly measure the height of shrubs and grasslands. The precise geographic coordinates and vegetation type information of each measurement point were also recorded. Throughout the data collection process, obstructions were avoided, and outliers were rechecked to ensure data reliability. Ultimately, validation data from 50 points were obtained, and the ground measurement data were compared with the CHM generated by the method proposed in this study. The accuracy verification results are detailed in Table 7.

CHM demonstrates high accuracy across various vegetation types, with a total mean absolute error (MAE) of 0.17 m and a relative error range of 0.27–6.21 %, achieving an overall accuracy of 95.03 %. Specifically, for non-ground vegetation, the MAE is 0.14 m, with a relative error range of 0.27–4.32 %, and an accuracy of 95.23 %, indicating that

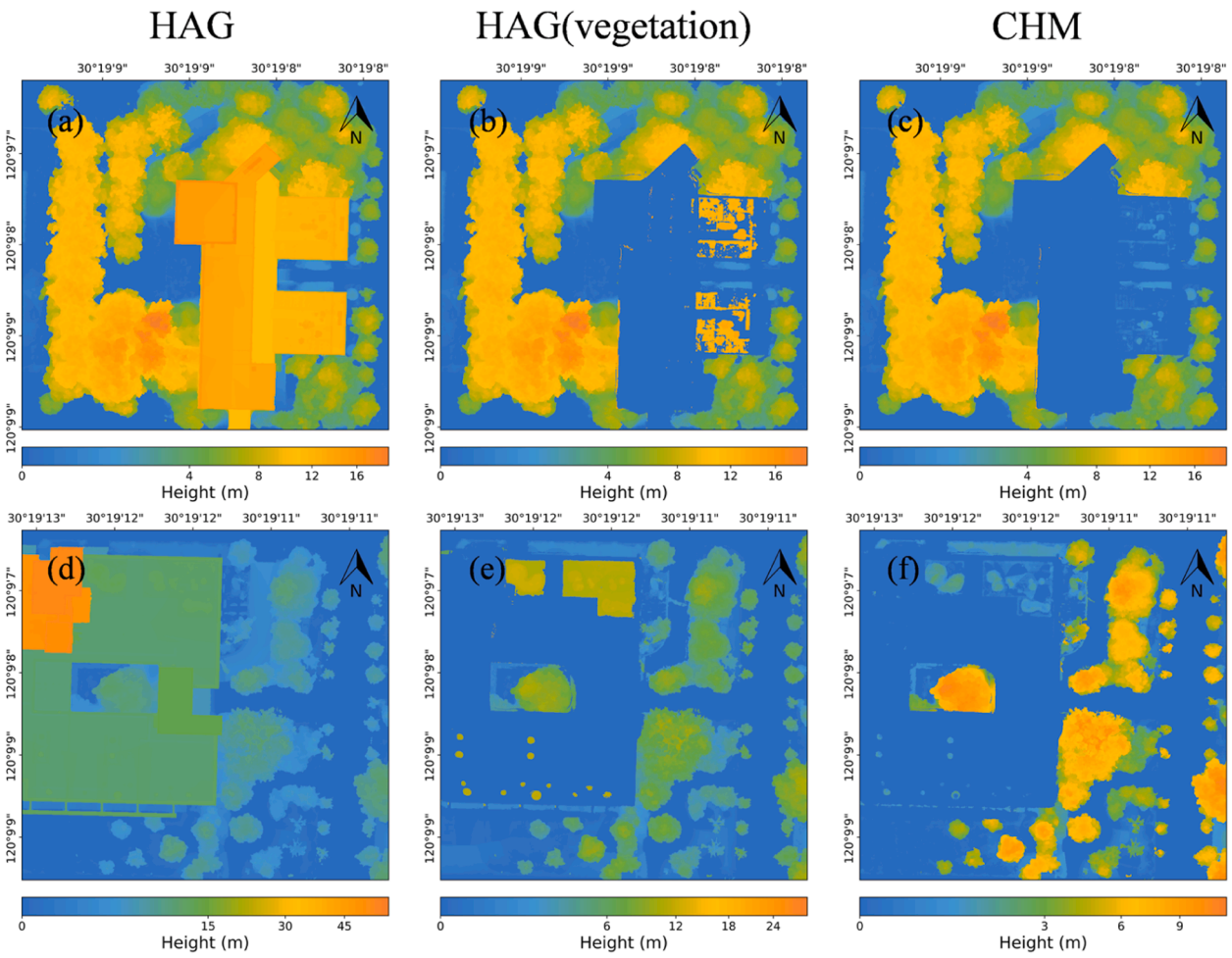

Fig. 3. Canopy height models where (a) and (d) show the above-ground height obtained by subtracting the DTM from the DSM, (c) and (e) retain only the height of the vegetation areas, and (c) and (f) represent the canopy height obtained by the method proposed in this paper.

Table 7
CHM accuracy verification results.

Type	Mean absolute error (m)	Relative error range (%)	Accuracy (%)
Ground vegetation	0.19	0.56 ~ 6.21	94.82
Non-ground vegetation	0.14	0.27 ~ 4.32	95.23
Total	0.17	0.27–6.21	95.03

CHM provides precise height estimates for non-ground vegetation. For ground vegetation, the mean absolute error is 0.19 m, with a relative error range of 0.56–6.21 %, and an accuracy of 94.82 %. Although the error is relatively higher, possibly due to factors such as terrain undulation, the overall accuracy remains at a high level. In general, CHM exhibits excellent reliability and meets research requirements. The main factors affecting the error include the resolution of UAV imagery, deviations in point cloud data processing, and interference from complex environments.

3.3. Vegetation classification accuracy evaluation

The results of classification accuracy for UGS vegetation using different feature subsets are presented in Table 8.

It can be noticed from Table 8 that spectral features (S1) resulted in an OA of 83.41 % and a Kappa coefficient of 0.75 which indicate low initial classification accuracy. When height information was introduced in S2, OA rose sharply to 93.77 % with an improvement of around 10 % demonstrating the importance of height information. However, by combining spectral features with VIs (S3), there is only a slight improvement, and the Kappa coefficient remained low (about 0.75). In contrast by incorporating texture features (S4), the Kappa coefficient became 0.77 which indicates that texture features contributed more to the classification process than VIs. When the height information was further incorporated, the classification performance improved again with the Kappa coefficient increasing to 0.90. The experimental results indicated that regardless of whether other features were combined, the classification accuracy in schemes where height information included was significantly higher than in those without height information.

However, when additional VIs (S5) and texture features (S6) were introduced into the RF classifier based on S2, the OA dropped to 93.75 % and 93.65 % respectively. This slight decline in accuracy suggests that the inclusion of redundant or less informative features may have introduced noise into the model, thereby reducing its performance. Even when all types of features were incorporated into the model in S8, optimal accuracy was not achieved. S9, which selected the optimal feature subset using the RFECV method, reached an OA of 93.82 % and a Kappa coefficient of 0.91, slightly higher than all other schemes, yielding significant classification results. The remaining inaccuracy of less than 10 % can be attributed to factors such as inherent spectral overlap between certain vegetation categories, limitations in spatial resolution, and potential misclassification of mixed objects at vegetation category boundaries. Table 8 shows that in some schemes, adding excessive VIs or texture features not only failed to improve classification

Table 8
Classification accuracies of schemes 1–9.

Class	S1		S2		S3		S4		S5		S6		S7		S8		S9	
	UA	PA	UA	PA	UA	PA	UA	PA	UA	PA	UA	PA	UA	PA	UA	PA	UA	PA
Grass	69.80	43.14	80.45	71.57	70.61	39.84	75.06	45.76	79.51	71.41	80.69	71.57	72.72	43.94	80.39	72.16	80.49	71.73
Shrub	79.55	25.79	79.36	60.75	80.73	26.91	80.73	24.77	79.76	61.87	80.21	60.75	80.51	25.28	80.13	62.48	79.50	62.48
Tree	90.29	96.61	96.21	97.97	89.94	96.80	90.44	97.00	96.23	97.85	96.19	97.83	90.37	96.95	96.20	97.83	96.30	97.83
Building	79.92	76.78	94.88	97.23	80.10	78.17	81.32	78.96	94.92	97.35	94.71	97.05	81.62	79.56	94.97	97.18	95.00	97.21
Background	77.27	81.77	92.49	92.20	77.93	81.57	78.80	82.76	92.52	92.13	92.12	92.12	79.15	82.89	92.52	92.24	92.47	92.38
OA	83.41		93.77		83.59		84.43		93.75		93.65		84.50		93.79		93.82	
Kappa	0.75		0.90		0.75		0.77		0.90		0.90		0.77		0.90		0.91	

accuracy but also led to performance degradation due to information redundancy.

In all experimental schemes, the PA and UA for the tree category were consistently higher than for other categories, with the PA approaching 1 and the UA remaining stable. This high accuracy is likely due to the distinct spectral and structural characteristics of trees, which make them easier to differentiate from other vegetation types. As more features were added, the classification accuracy for the shrub category showed the most notable improvement. When only spectral features were used, the PA for this category was 25.79 %, nevertheless after adding height information and other features, the PA increased to a maximum of 62.48 %. Nonetheless, the increase in features did not have the same impact on all categories, and for some categories, classification accuracy did not improve significantly with the addition of more features. This could be due to the inherent spectral and structural similarities between these categories and their surrounding environments, making them more challenging to classify even with additional features.

3.4. Feature importance

In this paper, 48 features were extracted where their contributions to vegetation classification varied while the most critical features for classification were selected using RFECV. As shown in Fig. 4, it can be noticed that with 17 feature variables, the OA reached 93.77 %, and the Kappa coefficient reached 0.90. Hence, it can be said that by adding more features could not significantly improve accuracy which indicate that too many features can lead to data redundancy and overfitting.

The most important 17 features were identified as the optimal feature subset for UGS vegetation classification on the basis of RFECV results. From Table 9 it can be noticed that these features were selected from the original 48 features, including 7 spectral features, 3 texture features, 3 VI features, and 4 height features. The feature importance ranking based on Gini impurity highlighted the significant role of height information (Zhang and Yang, 2020); specifically, the mean values of the CHM and DSM ranked first and second, respectively, while the other height-related features (such as the standard deviations of CHM and DSM) were also retained. Among the spectral features, several band variability features, including the standard deviation of the blue band, were selected, indicating that band variability plays an important role in distinguishing vegetation types. Moreover, texture features (such as the energy and contrast of the blue band) and VI features (such as the standard deviation of $NDVI_{rededge}$ and the mean of SAVI) were included in the optimal feature set, demonstrating their valuable contribution to refining classification.

A comparison between the RF classification results employing all

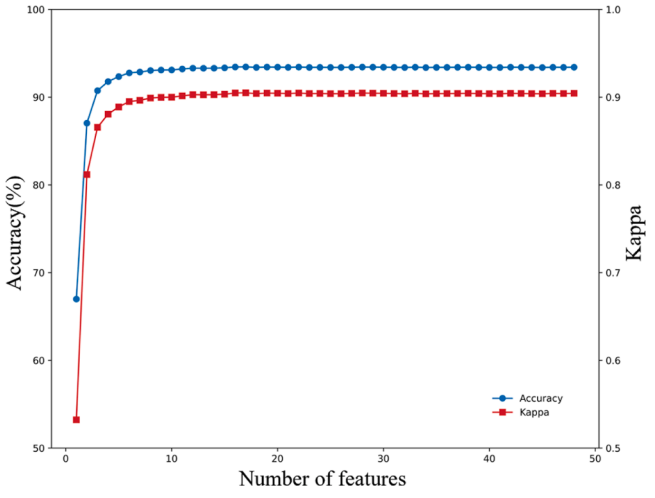

Fig. 4. Accuracy and kappa coefficient under different feature numbers.

Table 9
Optimized feature subset and feature importance ranking.

Ranking	Feature	Ranking	Feature
1	mean_chm	10	cor_g
2	mean_dsm	11	mean_savi
3	std_ndvi_rededge	12	mean_band1
4	std_b	13	std_band5
5	std_dsm	14	std_band1
6	std_savi	15	mean_band5
7	std_chm	16	std_g
8	ene_b	17	mean_band4
9	con_b		

features (S8) and those using the RFECV-selected optimal feature subset (S9) reveals slight differences in classification performance. When all features were used, the Kappa coefficient and OA were found to be 0.90 and 93.79 %, respectively and with the RFECV-selected feature subset, the Kappa coefficient increased to 0.91, and the OA rose to 93.82 %. The feature subset optimized by RFECV effectively reduced redundant information while retaining the most impactful features, leading to classification improvements across multiple categories. The PA for the grass category remained at 71.73 %, similar to previous results, but performance in other categories improved. Notably, the UA for the grass category increased slightly to 80.49 %, highlighting the effectiveness of feature selection. Although the overall performance of both approaches was similar, the RFECV feature selection method resulted in a slight improvement in classification accuracy. It enhanced the stability of UA in certain categories, and this underscores the importance of feature selection in identifying the optimal feature subset, which is essential for achieving multi-feature classification of UGS vegetation. It not only reduces model complexity but also improves classification accuracy.

3.5. *Classification result maps of the study area*

Fig. 5 presents the vegetation classification results of the study area via an object-based RF classifier across nine different feature subsets. Overall, all models were able to comprehensively identify UGS vegetation, but there were significant differences in the details. First, in areas where buildings and vegetation are intermingled, the models that did not use height features performed poorly and led to numerous misclassifications. For instance, some low shrubs or rooftop vegetation were mistakenly classified as trees, reducing classification accuracy. Moreover, confusion between background and building areas was noticeable, with many background objects being misclassified as buildings and building regions experiencing severe misclassification, which led to visible gaps in the classification result map; this misclassification affected the OA of the results while the models incorporating height features demonstrated significantly better classification results when compared to those without height features.

The introduction of height information allowed the classifier to better distinguish different types of vegetation, especially in complex urban environments, improving the recognition of trees and shrubs. In particular, the model using the RFECV-selected feature subset achieved the best classification performance, with vegetation distribution most closely matching the actual scenario, which underscores the importance of height features and feature selection in enhancing classification accuracy.

4. Discussion

The height information plays a crucial role in vegetation classification, reflecting the growth status of vegetation and its relationship with the environment. However, traditional CHM calculations often assume that all grown vegetation on the ground is not suitable for high-resolution UAV imagery in urban environments, especially with the increasing prevalence of rooftops and vertical greening, and this can lead to significant errors in vegetation height estimation, affecting classification and other applications (Fassnacht et al., 2021; Zhao et al., 2021). In order to handle this problem, this paper proposed a method to generate a CHM for UGS based on dual-source UAV RS images employing an innovative height correction algorithm to effectively resolve height errors associated with non-ground vegetation. While comparing the proposed framework to traditional methods, the CHM generated by the proposed approach eliminates the interference from non-vegetation areas and retains more accurate vegetation height information, resulting in enormous improvements in the accuracy of subsequent tasks.

The employment of various features extracted from UAV dual-source imagery is significant for UGS vegetation classification. In remote sensing research, there is widespread interest in the contribution of different features to classification performance. Several research studies introduced multiple features into a single classifier to assess their contributions by examining changes in overall classification accuracy (Neyns and Canters, 2022). This paper evaluated the importance of various features in UGS vegetation classification using RF model. The experimental results indicated that the inclusion of spectral features, canopy height information, VIs, and texture features all contributed to varying degrees of improving classification accuracy, and all types of features positively impacted the vegetation classification process. Although spectral features play an essential role, relying solely on spectral information does not provide sufficient discriminatory power in complex urban environments. A comprehensive feature selection strategy that combines height, texture, and VI information is an effective approach to improve classification accuracy.

The results provided in Table 8 show that when height information was introduced (S2), the classification accuracy improved by approximately 10 % compared to using only spectral features (S1), demonstrating the critical role of height information in classification performance. Hence, it's validated that the models incorporating height information achieved higher accuracy in all schemes than those without height features, and it indicates that height information is essential for distinguishing UGS vegetation types at the species level.

Although adding more feature types tends to increase classification accuracy, having too many features can also result in redundancy, which can lower classification accuracy and efficiency (Dhal and Azad, 2022). Feature redundancy typically arises from overlapping information between different features, which can degrade model performance rather than provide additional useful information. This study employed the RFECV method to optimize feature selection by identifying and eliminating features that contribute less to classification. Moreover, the feature subset selected by RFECV not only improved the accuracy of UGS vegetation classification but also significantly reduced computational overhead, and it suggests that in complex urban vegetation classification tasks, an appropriate feature selection strategy can maintain high accuracy while improving the efficiency of the model by providing more precise and efficient tools for urban vegetation monitoring and mapping.

The DTM rapid generation method employed in this study is primarily suitable for research areas with flat terrain and gradual elevation changes, and has certain application limitations in regions with significant topographic relief. Specifically, the applicability of the IDW interpolation method is limited in such complex terrains. The IDW method is based on the fundamental assumption of the "First Law of Geography," which posits that points closer in space are more similar. However, in areas with significant topographic variations and complex surface cover types (such as buildings, vegetation, etc.), this spatial autocorrelation assumption often does not hold. This limitation may lead to systematic errors in the DTM generation process, manifesting as overestimation or underestimation of topographic features, thereby affecting the accuracy of subsequent land cover classification. Therefore, it is necessary to consider more precise interpolation methods for regions with complex terrain. Additionally, the construction method of the CHM relies on the accuracy of vegetation extraction. Although VI

Fig. 5. Vegetation classification map of the study area.

methods are simple to calculate and widely used, they may have limitations in terms of accuracy. Therefore, exploring improved methods to enhance vegetation extraction accuracy would be beneficial for downstream tasks. The method proposed in this study achieved good classification results within the experimental area, but its broad applicability still needs further validation. The urban structure and vegetation types in the study area are relatively specific, and the environmental characteristics of other cities may differ, impacting the effectiveness of the method. Future research should conduct comparative experiments in different cities and ecosystems to verify the generalizability and adaptability of the method. Satellite imagery offers broader spatial coverage and, through multi-temporal analysis, provides valuable temporal insights (Orusa et al., 2024; Viani et al., 2024a). In the future, integrating similar technologies with satellite remote sensing data could significantly enhance the urban vegetation mapping process. Moreover, further exploration of its potential applications in climate regulation, carbon sequestration assessment, and environmental monitoring is needed to enhance its practical value in urban planning and ecological management.

5. Conclusion

To efficiently map UGS vegetation, the proposed study achieved the effectiveness of high-resolution UAV multi-spectral imagery combined with oblique photography imagery. Firstly, this study proposed a method for generating a CHM of UGS based on UAV dual-source remote sensing imagery, which effectively addresses the unique characteristics of urban greening. Secondly, an object-based classification method integrating multiple features was adopted to evaluate the contribution of different feature types to UGS vegetation classification. The key findings of the study include: (1) The vegetation canopy height correction algorithm based on dual-source imagery addressed the issue of large height errors for non-ground vegetation in previous CHM calculations. The CHM of UGS constructed in this study more accurately reflected actual vegetation height information, achieving a total MAE of 0.17 m and an overall accuracy of 95.03 %. (2) The experimental results demonstrated the critical role of height information in improving classification accuracy. The classification overall accuracy (OA) in the study area reached 93.82 %, with a kappa coefficient of 0.91. (3) The combination of rich spectral information from multi-spectral imagery and precise spatial information from oblique photography provides a more comprehensive description of vegetation features, contributing to improved classification accuracy.

Overall, the CHM generation and classification method based on UAV dual-source RS imagery showed significant potential for improving the accuracy of UGS vegetation classification. This paper provides an important breakthrough in terms of theoretical and technical support for urban planning, ecological management, and biodiversity conservation to contribute towards sustainable urban development. Future research may improve classification outcomes by integrating multi-source satellite remote sensing data and refining feature fusion algorithms. Moreover, extending this methodology to diverse urban environments, alongside systematic error analysis and uncertainty evaluation, will facilitate a more profound comprehension of its applicability and dependability. Concurrently, delving deeper into the potential applications of this method in monitoring wetland ecosystems and evaluating carbon sequestration dynamics could offer significant technical underpinnings for ecological and environmental governance.

CRediT authorship contribution statement

Ablameyko Sergey: Supervision, Resources, Investigation, Formal analysis, Conceptualization. **Ye Shiping:** Writing – review & editing, Supervision, Resources, Project administration, Funding acquisition, Formal analysis, Conceptualization. **Bai Zhican:** Visualization, Validation, Investigation, Formal analysis, Data curation. **Ye Chao:** Visualization, Validation, Software, Investigation, Formal analysis. **Li Ronghua:** Writing – review & editing, Writing – original draft, Visualization, Validation, Software, Methodology, Investigation.

Declaration of Competing Interest

The authors declare that they have no known competing financial interests or personal relationships that could have appeared to influence the work reported in this paper.

Acknowledgements

This research was funded by the Ministry of Science and Technology of the People's Republic of China (Grant Number: G2023016002L) and Ministry of Human Resources and Social Security of the People's Republic of China (Grant Number: H20240330).

References

Behera, T.K., Bakshi, S., Sa, P.K., 2023. A lightweight deep learning architecture for vegetation segmentation using UAV-captured aerial images. Sust. Comput. 37, 100841. https://doi.org/10.1016/j.suscom.2022.100841.

Belgiu, M., Drăguţ, L., 2016. Random forest in remote sensing: a review of applications and future directions. ISPRS J. Photogramm. Remote Sens. 114, 24–31. https://doi.org/10.1016/j.isprsjprs.2016.01.011.

Bhatnagar, S., Gill, L., Ghosh, B., 2020. Drone image segmentation using machine and deep learning for mapping raised bog vegetation communities. Remote Sens. 12 (16), 2602. https://doi.org/10.3390/rs12162602.

Che, Y., Wang, Q., Xie, Z., Zhou, L., Li, S., Hui, F., Wang, X., Ma, Y., 2020. Estimation of maize plant height and leaf area index dynamics using an unmanned aerial vehicle with oblique and nadir photography. Ann. Bot. 126 (4), 765–773. https://doi.org/10.1093/aob/mcaa097.

Chen, W., Huang, H., Dong, J., Zhang, Y., Tian, Y., Yang, Z., 2018. Social functional mapping of urban green space using remote sensing and social sensing data. ISPRS J. Photogramm. Remote Sens. 146, 436–452. https://doi.org/10.1016/j.isprsjprs.2018.10.010.

Chen, B., Nie, Z., Chen, Z., Xu, B., 2017. Quantitative estimation of 21st-century urban greenspace changes in Chinese populous cities. Sci. Total Environ. 609, 956–965. https://doi.org/10.1016/j.scitotenv.2017.07.238.

Chiang, S.H., Valdez, M., 2019. Tree species classification by integrating satellite imagery and topographic variables using maximum entropy method in a mongolian forest. Forests 10 (11), 961. https://doi.org/10.3390/f10110961.

Dai, W., Na, J., Huang, N., Hu, G., Yang, X., Tang, G., Xiong, L., Li, F., 2020. Integrated edge detection and terrain analysis for agricultural terrace delineation from remote sensing images. Int. J. Geogr. Inf. Sci. 34 (3), 484–503. https://doi.org/10.1080/13658816.2019.1650363.

Dhal, P., Azad, C., 2022. A comprehensive survey on feature selection in the various fields of machine learning. Appl. Intell. 52 (4), 4543–4581. https://doi.org/10.1007/s10489-021-02550-9.

Di, S., Li, Z.L., Tang, R., Pan, X., Liu, H., Niu, Y., 2019. Urban green space classification and water consumption analysis with remote-sensing technology: a case study in Beijing, China. Int. J. Remote Sens. 40 (5-6), 1909–1929. https://doi.org/10.1080/01431161.2018.1479798.

Fassnacht, F.E., Poblete-Olivares, J., Rivero, L., Lopatin, J., Ceballos-Comisso, A., Galleguillos, M., 2021. Using Sentinel-2 and canopy height models to derive a landscape-level biomass map covering multiple vegetation types. Int. J. Appl. Earth Obs. 94, 102236. https://doi.org/10.1016/j.jag.2020.102236.

Feng, Q., Liu, J., Gong, J., 2015. UAV remote sensing for urban vegetation mapping using random forest and texture analysis. Remote Sens. 7 (1), 1074–1094. https://doi.org/10.3390/rs70101074.

Franklin, S.E., Hall, R.J., Moskal, L.M., Maudie, A.J., Lavigne, M.B., 2000. Incorporating texture into classification of forest species composition from airborne multi-spectral images. Int. J. Remote Sens. 21 (1), 61–79. https://doi.org/10.1080/014311600210993.

Gašparović, M., Dobrinić, D., 2020. Comparative assessment of machine learning methods for urban vegetation mapping using multitemporal sentinel-1 imagery. Remote Sens. 12 (12), 1952. https://doi.org/10.3390/rs12121952.

Gillan, J.K., Karl, J.W., Duniway, M., Elaksher, A., 2014. Modeling vegetation heights from high resolution stereo aerial photography: an application for broad-scale rangeland monitoring. J. Environ. Manag. 144, 226–235. https://doi.org/10.1016/j.jenvman.2014.05.028.

Granholm, A.H., Olsson, H., Nilsson, M., Allard, A., Holmgren, J., 2015. The potential of digital surface models based on aerial images for automated vegetation mapping. Int. J. Remote Sens. 36 (7-8), 1855–1870. https://doi.org/10.1080/01431161.2015.1029094.

Haralick, R.M., Shanmugam, K., Dinstein, I.H., 1973. Textural features for image classification. IEEE Trans. Syst. Man Cyber 6, 610–621. https://doi.org/10.1109/TSMC.1973.4309314.

HARIF, A., KASSIMI, M.A., 2024. Predictive modeling of student performance using RFECV-RF for feature selection and machine learning techniques. Int. J. Adv. Comput. Sci. Appl. 15 (7). https://doi.org/10.14569/IJACSA.2024.0150723.
Huete, A.R., 1988. A soil-adjusted vegetation index (SAVI). Remote Sens. Environ. 25 (3), 295–309. https://doi.org/10.1016/0034-4257(88)90106-X.
Huete, A., Didan, K., Miura, T., Rodriguez, E.P., Gao, X., Ferreira, L.G., 2002. Overview of the radiometric and biophysical performance of the MODIS vegetation indices. Remote Sens. Environ. 83 (1-2), 195–213. https://doi.org/10.1016/S0034-4257(02)00096-2.
Jiang, B., Chen, W., Zou, Y., Wu, C., Wu, Z., Kang, X., Xiao, H., Sakai, T., 2024. Post-fire vegetation dynamic patterns and drivers in greater Hinggan Mountains: insights from long-term remote sensing data analysis. Ecol. Inf., 102850 https://doi.org/10.1016/j.ecoinf.2024.102850.
Katz, D.S.W., Batterman, S.A., Brines, S.J., 2020. Improved classification of urban trees using a widespread multi-temporal aerial image dataset. Remote Sens. 12 (15), 2475. https://doi.org/10.3390/rs12152475.
Komárek, J., Klouček, T., Prošek, J., 2018. The potential of unmanned aerial systems: a tool towards precision classification of hard-to-distinguish vegetation types? Int. J. Appl. Earth Obs. Geoinf. 71, 9–19. https://doi.org/10.1016/j.jag.2018.05.003.
Kopecká, M., Szatmári, D., Rosina, K., 2017. Analysis of urban green spaces based on Sentinel-2A: Case studies from Slovakia. Land 6 (2), 25. https://doi.org/10.3390/land6020025.
Kothencz, G., Kulessa, K., Anyyeva, A., Lang, S., 2018. Urban vegetation extraction from vhr (tri-)stereo imagery – a comparative study in two central european cities. Eur. J. Remote Sens. 51 (1), 285–300. https://doi.org/10.1080/22797254.2018.1431057.
Li, R., Ye, S., Bai, Z., Nedzved, A., Tuzikov, A., 2024. Moderate Red-Edge vegetation index for High-Resolution multi-spectral remote sensing images in urban areas. Ecol. Indic. 167, 112645. https://doi.org/10.1016/j.ecolind.2024.112645.
Lisein, J., Pierrot-Deseilligny, M., Bonnet, S., Lejeune, P., 2013. A photogrammetric workflow for the creation of a forest canopy height model from small unmanned aerial system imagery. Forests 4 (4), 922–944. https://doi.org/10.3390/f4040922.
Liu, L., Coops, N.C., Aven, N.W., Pang, Y., 2017. Mapping urban tree species using integrated airborne hyperspectral and lidar remote sensing data. Remote Sens. Environ. 200, 170–182. https://doi.org/10.1016/j.rse.2017.08.010.
Liu, Z.N., Yu, X.Y., Jia, L.F., Wang, Y.S., Song, Y.C., Meng, H.D., 2021. The influence of distance weight on the inverse distance weighted method for ore-grade estimation. Sci. Rep. 11 (1), 2689. https://doi.org/10.1038/s41598-021-82227-y.
Murray, H., Lucieer, A., Williams, R., 2010. Texture-based classification of sub-antarctic vegetation communities on heard island. Int. J. Appl. Earth Obs. Geoinf. 12 (3), 138–149. https://doi.org/10.1016/j.jag.2010.01.006.
Nero, B.F., 2017. Urban green space dynamics and socio-environmental inequity: multi-resolution and spatiotemporal data analysis of Kumasi, Ghana. Int. J. Remote Sens. 38 (23), 6993–7020. https://doi.org/10.1080/01431161.2017.1370152.
Neyns, R., Canters, F., 2022. Mapping of urban vegetation with high-resolution remote sensing: a review. Remote Sens. 14 (4), 1031. https://doi.org/10.3390/rs14041031.
Onishi, M., Ise, T., 2021. Explainable identification and mapping of trees using uav rgb image and deep learning. Sci. Rep. 11 (1). https://doi.org/10.1038/s41598-020-79653-9.
Orusa, T., Viani, A., Borgogno-Mondino, E., 2024. Earth observation data and geospatial deep learning AI to assign contributions to European municipalities Sen4MUN: an empirical application in Aosta Valley (NW Italy). Land 13 (1), 80. https://doi.org/10.3390/land13010080.
Prošek, J., Šímová, P., 2019. UAV for mapping shrubland vegetation: does fusion of spectral and vertical information derived from a single sensor increase the classification accuracy? Int. J. Appl. Earth Obs. Geoinf. 75, 151–162. https://doi.org/10.1016/j.jag.2018.10.009.
Pu, R., Landry, S., Yu, Q., 2011. Object-based urban detailed land cover classification with high spatial resolution IKONOS imagery. Int. J. Remote Sens. 32 (12), 3285–3308. https://doi.org/10.1080/01431161003745657.
Radke, D., Radke, D., Radke, J., 2020. Beyond measurement: extracting vegetation height from high resolution imagery with deep learning. Remote Sens. 12 (22), 3797. https://doi.org/10.3390/rs12223797.
Richards, D.R., Belcher, R.N., 2019. Global changes in urban vegetation cover. Remote Sens. 12 (1), 23. https://doi.org/10.3390/rs12010023.
Rouse, J.W., Haas, R.H., Schell, J.A., Deering, D.W., 1974. Monitoring vegetation systems in the Great Plains with ERTS. NASA Spec. Publ. 351 (1), 309.
Sathyakumar, V., Ramsankaran, R.A.A.J., Bardhan, R., 2019. Linking remotely sensed urban green space (UGS) distribution patterns and socio-economic status (SES)-a multi-scale probabilistic analysis based in Mumbai, India. Gisci. Remote Sens. 56 (5), 645–669. https://doi.org/10.1080/15481603.2018.1549819.
Shahtahmassebi, A.R., Li, C., Fan, Y., Wu, Y., Gan, M., Wang, K., Malik, A., Blackburn, G. A., 2021. Remote sensing of urban green spaces: a review. Urban For. Urban Green. 57, 126946. https://doi.org/10.1016/j.ufug.2020.126946.
Shi, S., Bi, S., Gong, W., Chen, B., Chen, B., Tang, X., Qu, F., Song, S., 2021. Land cover classification with multi-spectral LiDAR based on multi-scale spatial and spectral feature selection. Remote Sens. 13 (20), 4118. https://doi.org/10.3390/rs13204118.
Snavely, R.A., Uyeda, K.A., Stow, D.A., O'Leary, J.F., Lambert, J., 2019. Mapping vegetation community types in a highly disturbed landscape: integrating hierarchical object-based image analysis with lidar-derived canopy height data. Int. J. Remote Sens. 40 (11-12), 1–17. https://doi.org/10.1080/01431161.2018.1562588.
Sotille, M.E., Bremer, U.F., Vieira, G., Velho, L.F., Petsch, C., Simões, J.C., 2020. Evaluation of UAV and satellite-derived NDVI to map maritime Antarctic vegetation. Appl. Geogr. 125, 102322. https://doi.org/10.1016/j.apgeog.2020.102322.
Timmer, B., Reshitnyk, L.Y., Hessing-Lewis, M., Juanes, F., Costa, M., 2022. Comparing the use of red-edge and near-infrared wavelength ranges for detecting submerged kelp canopy. Remote Sens. 14 (9), 2241. https://doi.org/10.3390/rs14092241.
Viani, A., Orusa, T., Borgogno-Mondino, E., Orusa, R., 2024a. A one health google earth engine web-GIS application to evaluate and monitor water quality worldwide. Eur. Mediterr. J. Environ. Integr. 1–14. https://doi.org/10.1007/s41207-024-00528-w.
Viani, A., Orusa, T., Mandola, M.L., Robetto, S., Nogarol, C., Mondino, E.B., Orusa, R., 2024b. Grading habitats for ticks by mapping a suitability index based on remotely sensed data and Meta® population dataset in Aosta Valley, NW Italy. Vet. Ital. 60 (4). https://doi.org/10.12834/VetIt.3481.24368.2.
Wang, Y., Jin, S., Dardanelli, G., 2024. Vegetation classification and evaluation of yancheng coastal wetlands based on random forest algorithm from sentinel-2 images. Remote Sens. 16 (7), 1124. https://doi.org/10.3390/rs16071124.
Wang, X., Meng, Q., Zhang, L., Hu, D., 2021. Evaluation of urban green space in terms of thermal environmental benefits using geographical detector analysis. Int. J. Appl. Earth Obs. Geoinf. 105, 102610. https://doi.org/10.1016/j.jag.2021.102610.
Watson, D.F., 1985. A refinement of inverse distance weighted interpolation. Geo Process. 2, 315–327.
Xie, Z., Chen, Y., Lu, D., Li, G., Chen, E., 2019. Classification of land cover, forest, and tree species classes with ZiYuan-3 multi-spectral and stereo data. Remote Sens. 11 (2), 164. https://doi.org/10.3390/rs11020164.
Xu, Z.Y., Zhou, Y., Wang, S.X., Wang, L., Li, F., Wang, S., Wang, Z., 2020. A novel intelligent classification method for urban green space based on high-resolution remote sensing images. Remote Sens. 12. https://doi.org/10.3390/rs12223845.
Yang, J., Guan, Y., Xia, J.C., Jin, C., Li, X., 2018. Spatiotemporal variation characteristics of green space ecosystem service value at urban fringes: a case study on Ganjingzi District in Dalian, China. Sci. Total Environ. 639, 1453–1461. https://doi.org/10.1016/j.scitotenv.2018.05.253.
Yu, X., Lu, D., Jiang, X., Li, G., Chen, Y., Li, D., Chen, E., 2020. Examining the roles of spectral, spatial, and topographic features in improving land-cover and forest classifications in a subtropical region. Remote Sens. 12 (18), 2907. https://doi.org/10.3390/rs12182907.
Zhang, F., Yang, X., 2020. Improving land cover classification in an urbanized coastal area by random forests: the role of variable selection. Remote Sens. Environ. 251, 112105. https://doi.org/10.1016/j.rse.2020.112105.
Zhao, D., Cai, J., Xu, Y., Liu, Y., Yao, M., 2023. Carbon sinks in urban public green spaces under carbon neutrality: a bibliometric analysis and systematic literature review. Urban For. Urban Green., 128037 https://doi.org/10.1016/j.ufug.2023.128037.
Zhao, S., Jiang, X., Li, G., Chen, Y., Lu, D., 2021. Integration of ZiYuan-3 multi-spectral and stereo imagery for mapping urban vegetation using the hierarchy-based classifier. Int. J. Appl. Earth Obs. Geoinf. 105, 102594. https://doi.org/10.1016/j.jag.2021.102594.
Zhuang, Q., Shao, Z., Gong, J., Li, D., Huang, X., Zhang, Y., Xu, X., Dang, C., Chen, J., Altan, O., Wu, S., 2022. Modeling carbon storage in urban vegetation: progress, challenges, and opportunities. Int. J. Appl. Earth Obs. 114, 103058. https://doi.org/10.1016/j.jag.2022.103058.